CHAPTER III

INFLUENCE OF IRRADIATION PARAMETERS ON MASS SPECTRA

3.1. Introduction

The matrix-assisted laser desorption-ionization (MALDI) technique, pioneered by Hillenkamp and Karas [2-5], has become a popular method for ejecting large, thermally labile, non-volatile molecules from condensed phases into the gas phase as ions. The basic principle of the MALDI technique, namely, "soft" desorption and ionization of analyte molecules using a matrix as an intermediate medium for absorbing laser radiation, is well established empirically [4-6] and, to some extent, quantitatively [7-10]. Even though the details of the MALDI process are still actively debated, MALDI is widely used for mass analysis of biomolecules, carbohydrates [11], polymers [12], and hazardous waste components [13,14] and new developments, such as zeptomole sampling [15], continue to be driven empirically. However, the complications resulting from the use of different wavelengths [16-19], laser pulse durations [18,20-22], matrix preparations [23-26] and ion extraction parameters [27,28] have made it difficult to develop mechanistic models that comprehend the great variety of experimental observations.

Among the many studies of MALDI mechanisms are a number that exhibit remarkably similar mass spectra for many wavelengths [29,30] and for both nanosecond and femtosecond pulse durations [20]. In fact, Siegal *et al*. have demonstrated that mass spectra of a given species seem to be independent not only of laser wavelength but even ionization techniques [16]. These observations have sometimes been interpreted as evidence for a single MALDI mechanism operative at all wavelength regimes and laser pulse durations. Such a strong conclusion, however, seems unwarranted without systematic experiments, particularly since one knows from first principles that the initial phase of the laser-solid interaction differs substantially in electronic and vibrational excitation density depending on laser wavelength and pulse duration.

Our experiments, recently published [31], used laser sources covering the broadest yet reported range of UV and IR excitation wavelengths and pulse durations, allowing us to compare mass spectra from the same types of matrix-analyte systems under widely varying conditions of

laser-solid interaction mechanisms, laser intensity and fluence. Our discussion of the ion-formation mechanism in MALDI considers the plausibility of multiphoton ionization, the possible role of excited-state charge transfer, the contribution of laser-plume interactions and the differences between electronically and vibrationally excited MALDI systems. Our results appear to restrict the possible roles of multiphoton ionization and laser-induced plume ionization, and may also cast doubt on the general validity of ion formation mechanisms involving matrix excited states. These similarities can be explained if the observed ions instead reflect the gas-phase properties of the analyte. If the early stages of the plume evolution occur in thermodynamic equilibrium, then provided there are sufficient ions present, regardless of their identity and history, the most basic species will preferentially emerge as the charged (protonated) species in positive ion mass spectra. This hypothesis has been found to agree with the relative basicity values of analyte and matrix molecules as they have become available. In this model, the particular irradiation wavelength is unimportant, provided that: (1) a phase transition is accomplished and (2) ions are generated prior to or during that transition and (3) sufficient collisions occur to allow equilibrium to be established.

Table 3.1: Lasers Used in UV- and IR- MALDI Experiments

Laser Type	Wavelength	Pulse Duration	Energy/Pulse
Nd:YAG[1]	266 nm (4ω)	2 ns	0.25-5.0 mJ
N_2[2]	337 nm	3 ns	600 μJ
Ti:sapphire[3]	400 nm, 266 nm (2 ω, 3 ω)	120 fs	3 mJ, 2 mJ
Free-electron laser[4]	2-10 μm continuously tunable	micropulse ~1 ps macropulse 4 μs	micropulse ~2 μJ macropulse ~600 μJ

[1] Coherent, Inc., 5100 Patrick Henry Drive, Santa Clara, CA 95054. Infinity Nd:YAG.
[2] Laser Science, Inc., 8E Forge Parkway, Franklin, MA 02038. Model VSL-337.
[3] Spectra Physics, Mountain View, CA. Tsunami oscillator with Spitfire regenerative amplifier and harmonic generation.
[4] For a description of the Vanderbilt free-electron laser system, see Reference [1].

3.2. Experimental Procedures

The general experimental parameters utilized in this chapter are described more fully in Chapter 2, but selected details are included here. All experiments were performed on commercial MALDI reflectron time-of-flight (TOF) mass spectrometers that were modified to accept laser pulses from multiple external laser sources. The UV mass spectra represent an average of 15-20 shots, while the IR spectra are 10-shot averages. The laser systems used in our experiments, listed in Table 3.1, covered a broad range of wavelengths and pulse durations. For the IR-MALDI experiments, the FEL was tuned to two different absorption bands, chosen from FTIR absorption spectra to take advantage of strong C=O and OH vibrational modes of the matrix. The laser spot size on the sample was ~200 μm in diameter for both the ultraviolet and infrared studies.

The fluence used for all the experiments was chosen to be slightly above the analyte ion signal threshold to obtain a good signal-to-noise ratio with reasonable reproducibility. This

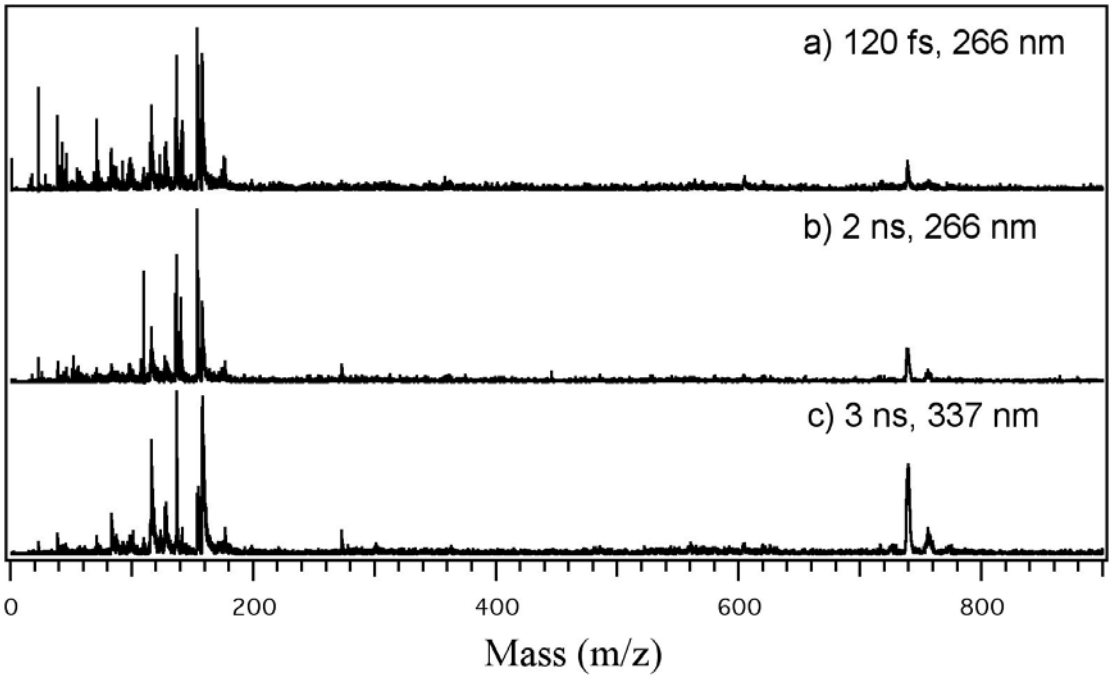

Figure 3.1. UV-MALDI mass spectra of erythromycin in 2,5 dihydroxybenzoic acid (1:100 molar ratio) comparing two different time domains: a) femtosecond, and b) nanosecond and wavelengths: b) 266 nm and c) 337 nm. The lower mass portion of the spectra is dominated by matrix and fragmentation peaks. In the analyte mass region consists of the parent peak, $[\text{erythromycin+H}]^+$, and a smaller $[\text{erythromycin+Na}]^+$ peak. The intensity scales are similar for each spectrum.

threshold at UV wavelengths was ~50 mJ cm^{-2}, for the IR studies fluences of 130 mJ cm^{-2} (5.9 μm) and 670 mJ cm^{-2} (2.8 μm) were used. However, due to the more efficient extinction of the Pockels cell at 5.9 μm compared to 2.8 μm, the micropulse *intensities* in both cases were closer than indicated by the difference in the fluence values.

Samples were prepared by mixing 2,5-dihydroxybenzoic (DHB) acid (Aldrich, Milwaukee, WI, USA) with angiotensin II (Sigma, St. Louis, MO, USA), erythromycin or β-cyclodextrin (Aldrich, Milwaukee, WI, USA). DHB was chosen as a matrix because it functions well for a number of analytes, can be used in both the ultraviolet and infrared, and, as the best studied MALDI matrix material, more is known about its energetic and gas-phase properties. The angiotensin II and β-cyclodextrin were diluted in a 100:1 matrix:analyte molar ratio while the erythromycin was present at a 10:1 concentration, at the upper limit of MALDI experiments. A 1 μL drop of the mixture was then deposited in a sample well of a microtiter plate and dried in air, prior to insertion in the ion source.

The MALDI experiments reported here cover the widest range of wavelengths and pulse durations carried out until now. From these experiments, we have selected representative data that make possible some conclusions about the mechanisms of matrix-assisted desorption and ionization of the small peptides and oligosaccharides used as analytes for these model experiments. Although we shall continue to use the familiar MALDI acronym, it should be noted at the outset that this process is more properly called matrix-assisted laser *ablation*/ionization, as in all cases significant quantities of material are removed with each laser pulse. Because of the amount of material removed, it is crucial to take into account secondary processes occurring in the ablation plume, especially in experiments with nanosecond pulses. Our analysis focused on positive ion spectra, though we recognize that additional insights might be gleaned from a similar inspection of negative ion spectra.

3.3. Comparison of pulse duration on UV-MALDI mass spectra

Meaningful studies of pulse-duration effects in MALDI require comparisons of nanosecond and picosecond or femtosecond pulse effects, since once pulse durations exceed ~10 ps, energy is thermalized and the ablation process takes place in thermal equilibrium. Figures 3.1, 3.2 and 3.3 display mass spectra of erythromycin, ß-cyclodextrin and angiotensin II,

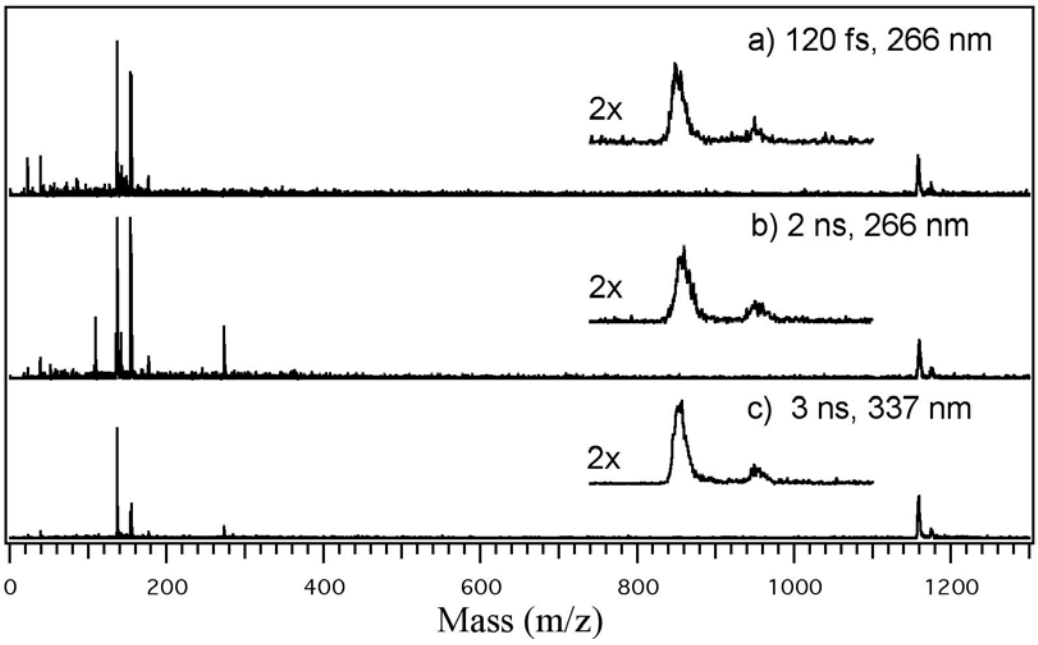

Figure 3.2. UV-MALDI mass spectra of ß-cyclodextrin in a DHB matrix for three different ionization conditions: (a) femtosecond 266 nm, (b) nanosecond 266 nm and (c) nanosecond 337 nm excitation. The enlarged portion of the analyte region clearly shows two mass peaks that represent salt adducts of the parent molecule: $[\text{ß-cyclodextrin} + \text{Na}]^+$ and $[\text{ß-cyclodextrin} + \text{K}]^+$, respectively. The intensity scales are the same for each spectrum.

respectively, in a 2,5-DHB matrix. For each sample, we compare the spectra generated by 266 nm irradiation at pulse lengths of 120 fs and 2 ns. In the mass region below m/z 300 Da., the spectra are dominated by alkali metal (sodium and potassium), matrix and matrix fragment peaks. Matrix peaks include protonated ($[\text{DHB} + \text{H}]^+$), radical ($\text{DHB}^{+\bullet}$), sodiated ($[\text{DHB} + \text{Na}]^+$) and sodium salt radical ($[\text{DHB} - \text{H} + \text{Na}]^{+\bullet}$) cations. The strongest matrix fragment peaks are due to losses of hydroxyl, water, and carboxyl groups from the parent 2,5-DHB compound, which has a molecular weight of 154. Additionally, a peak at m/z = 273, corresponding to a $[2\text{DHB} - \text{OH} - \text{H}_2\text{O}]^+$ ion, is present in several of the spectra.

The mass region above 300 Da consists of a protonated analyte peak with a smaller sodiated analyte peak for the DHB-erythromycin sample [Fig. 3.1(a) and (b)] and the DHB-angiotensin II sample [Fig. 3.2(c) and (d)]. The mass resolution is not sufficient to resolve radical and protonated analyte peaks, and we will henceforth refer to the analyte signals as protonated or sodiated. The dominant analyte mass peak for the DHB-ß-cyclodextrin spectra is $[\text{ß-cyclodextrin+Na}]^+$, while a smaller feature representing $[\text{ß-cyclodextrin+K}]^+$ is apparent [Fig. 3.2]. The protonated analyte peak is absent in these spectra. The absence of the

protonated mass peak is not surprising as MALDI of oligosaccharides tends to produce only alkali metal adducted mass peaks [12,32]. For the erythromycin spectra [Fig. 3.1(a) and (b)], the ratio of matrix to analyte intensities seems unchanged by the different pulse durations, whereas for angiotensin II the femtosecond spectrum [Fig. 3.3(d)] shows a lower matrix:analyte ratio than the nanosecond spectrum [Fig. 3.3(c)]. Detector saturation of the matrix signals for the ß-cyclodextrin spectra for the 266 nm nanosecond spectrum [Fig. 2(b)] prevents a definitive discussion of the matrix:analyte ratios, although they appear similar for both pulse durations. Taken together, these spectra do not show any trend in the data favoring either analyte or matrix production due to pulse duration effects. The fluence threshold for MALDI signal is similar for nanosecond and femtosecond pulses despite the fact that the irradiance differs by greater than a factor of $>10^4$. Our results are similar to earlier studies that also obtained nearly identical MALDI spectra using both ultrashort-pulse (< 1 ps) and longer pulse (>2 ns) lasers [20,21]. However, this is scarcely surprising since threshold is measured by ion yield, and this quantity is necessarily proportional to energy deposited per unit volume.

3.4. Comparison of excitation wavelength on mass spectra

The same matrix:analyte samples described above were irradiated using 337 and 266 nm nanosecond laser pulses. The absolute molar absorption of 2,5-DHB in the solid phase is not known for these two wavelengths, but reflectance spectroscopy indicates that 266 nm corresponds to a minimum in the absorption curve, 337 nm is near an absorption maximum, and 400 nm, to be discussed shortly, appears to be in a region of negligible absorption [33]. Figure 3.1 shows that similar spectra are obtained for 266 nm [Fig. 3.1(b)] and 337 nm [Fig. 3.1(c)], with the exception of a stronger analyte yield with respect to the matrix intensities for the 337 nm case. Figure 3.2 displays MALDI mass spectra of ß-cyclodextrin in DHB. In the 266 nm spectrum [Fig. 3.2(b)], the parent matrix peak and dehydroxylated peak are truncated owing to detector saturation, and the peaks corresponding to a decarboxylation fragment and a DHB cluster peak at *m/z* 273 appear comparatively stronger than those in the 337 nm spectrum [Fig. 3.2(c)]. However, even at the typical MALDI excitation wavelength of 337 nm [Fig. 3.2(c)], the analyte signal is nearly identical with nanosecond and femtosecond mass spectra. As noted above, the absence of the protonated mass peak is consistent with well-known

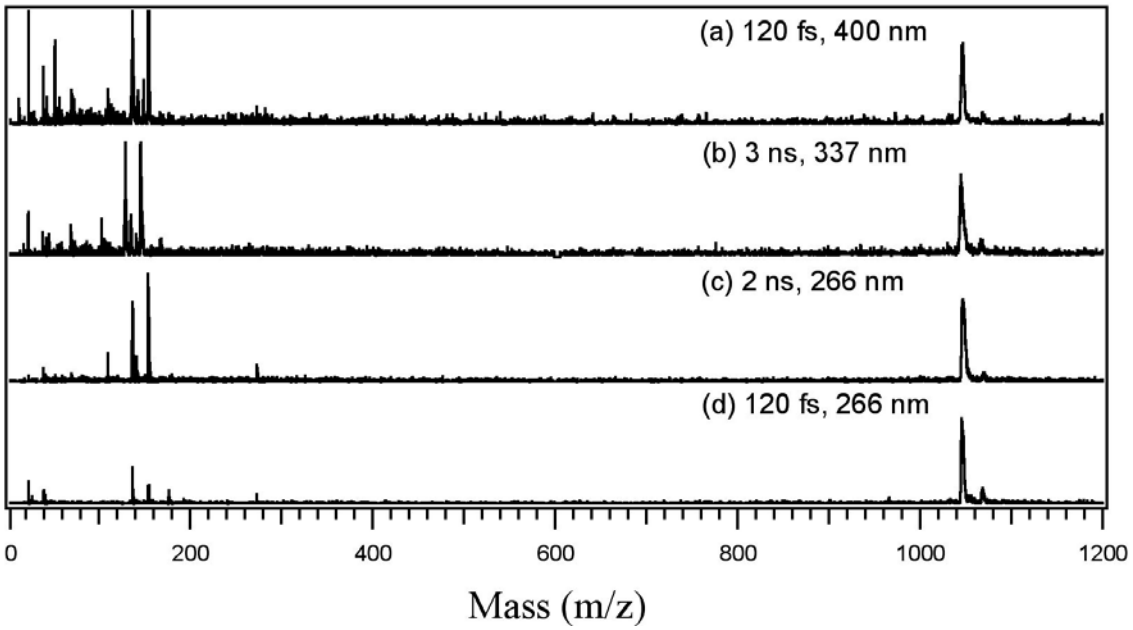

Figure 3.3. MALDI mass spectra of angiotensin II obtained under various ionization conditions: (a) femtosecond laser at 400 nm, (b) nanosecond laser at 337 nm, (c) nanosecond laser at 266 nm, (d) femtosecond laser at 266 nm. All samples (a-d) were prepared using a dried droplet method using 2,5-DHB matrix. The protonated angiotensin II molecule is the dominant feature in the high mass region (>1000 Da). The small peak, adjacent to the protonated analyte peak, is the [angiotensin II+Na]$^+$. The intensity scales are similar for each spectrum.

results for MALDI of oligosaccharides [12,32]. Figure 3.3 displays angiotensin II MALDI mass spectra obtained at excitation wavelengths of 400 nm [Fig. 3.3(a)] and 266 nm [Fig. 3.3(d)] using femtosecond pulses in addition to the comparisons of nanosecond 337 [Fig. 3.3(b)] and 266 nm [Fig. 3.3(c)] laser pulses. Detector saturation of some of the low-mass peaks again frustrates rigorous comparisons of the wavelength dependence, but we see that in both the femtosecond and nanosecond cases the longer wavelength spectrum shows a higher yield of low-mass signals, especially the alkali metal ions. As with the erythromycin and ß-cyclodextrin MALDI spectra, the analyte mass spectra are nearly identical under these widely varying conditions, with minor differences in the low-mass region of the spectra under different ionization conditions. The analyte mass spectra consist of an intense protonated angiontensin II peak with a smaller sodium-adduct feature ([angiotensin II + Na]$^+$).

Although the analyte mass region of the spectra appears relatively consistent in terms of resolution and degree of adduction for the three analyte systems studied under different ionization conditions, there are noticeable variations in the low-mass region. We examined this

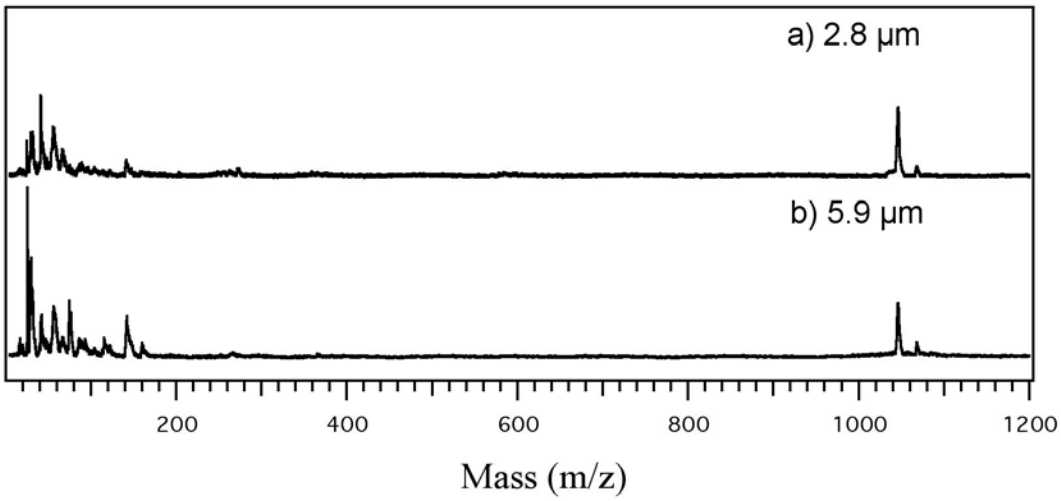

Figure 3.4. Infrared FEL MALDI mass spectra of angiotensin II in a DHB matrix at (a) 2.8 □m and (b) 5.9 μm. The main peak represents protonated angiotensin II with a smaller sodiated peak. The sample mixture is the same as used for the spectra in Fig. 3.3.

region for relationships between the spectra and irradiation conditions that might elucidate specific reaction pathways to ion formation. However, examination of the ion species present and the yield ratios of these species as a function of pulse duration and wavelength revealed no significant trend consistent for all three matrix-analyte systems studied suggesting such a pathway.

Figure 3.4 shows that MALDI mass spectra can be obtained across a wide range of photon energies in the IR (from 0.21 to 0.44 eV) at wavelengths resonant with particular vibrational modes of the 2,5-DHB matrix. However, it is not clear that strong bulk absorption is a requirement for efficient IR-MALDI, as some studies by our group and by others show strong MALDI signals in spectral regions of weak bulk absorption [14,19,24,34]. Moreover, even with the unusual temporal pulse structure of the FEL, there seems to be little difference in the final-state mass spectra compared to the mass spectra of the same ions obtained under UV excitation.

Figure 3.5 displays angiotensin II MALDI mass spectra excited using (a) a nanosecond nitrogen laser at 337 nm and (b) a picosecond FEL tuned to 5.9 μm Here we see that the matrix peaks are strongly suppressed, a phenomenon commonly called the matrix suppression effect. The spectrum in Fig. 3.5(a) was obtained using the same sample as presented in Fig. 3.3(b) by illuminating a different spot on the dried droplet. The matrix suppression effect in UV-MALDI, discussed further in Section 4.2.2, tends to be observed for low-mass analyte molecules under

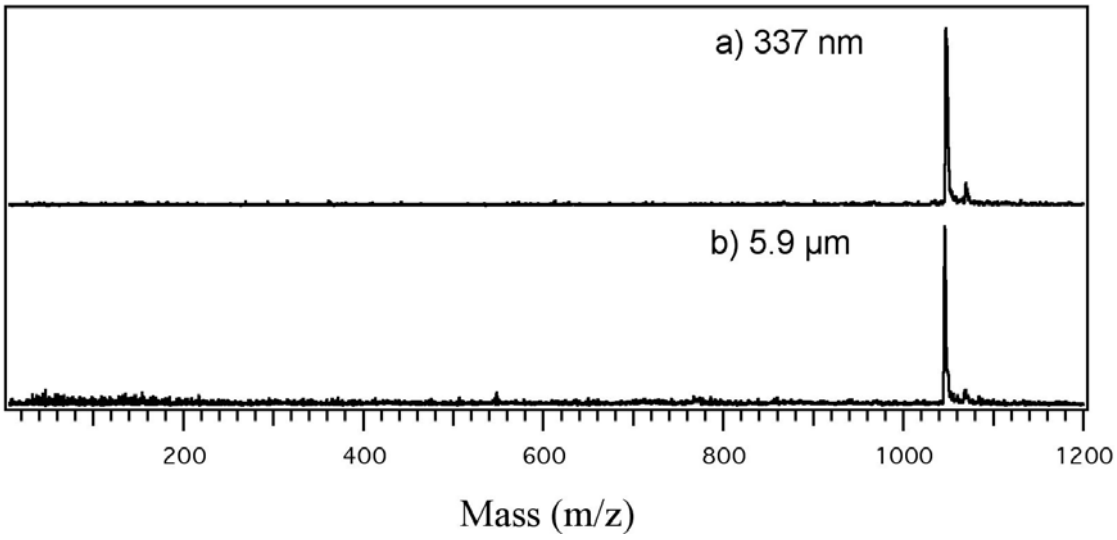

Figure 3.5. Mass spectrum of angiotensin II in 2,5-DHB showing matrix suppression using dried droplet preparations: a) with nanosecond 337 nm and b) picosecond 5.9 μm excitation. The two spectra, obtained on different instruments, have been scaled for clarity.

appropriate matrix:analyte concentration ratios. While spectra with strongly or completely suppressed matrix signals have been observed in IR spectra, to our knowledge no systematic study of the effect has been reported. Our unpublished observations are that the effect is sensitive to laser intensity and observed only at intensities just above the ion threshold. The sample morphology may also contribute to this effect. Clearly, the variation in the ion abundances observed in the matrix mass region can be dominated by seemingly minor differences in sample concentration and morphology.

3.5. The 'standard model' for primary ion formation in UV-MALDI

A MALDI experiment can be resolved conceptually into distinct stages. In the initial state, the laser deposits energy either into localized electronic or rovibronic degrees of freedom of the matrix, depending on laser wavelength; this energy is then thermalized by dissipation to the delocalized phonon modes. In principle, both the relaxation mechanism and time-scale of irradiation will have observable consequences for the formation of the ablation plume. The initial local density of electronic or vibrational excitation also depends on the absorption coefficient of the matrix, which may include a nonlinear or intensity-dependent term that will have observable effects for picosecond or femtosecond laser pulses at intensities above some

threshold. The absorption of the matrix may also depend on the density of defects within the matrix or on the surface. Indeed, the standard MALDI "dried droplet" preparation produces a substrate that is egregiously defective, a fact that has hitherto rarely been considered in MALDI studies.

The intermediate state in a MALDI experiment involves the formation of a plume overwhelmingly dominated by matrix and analyte neutrals, with a tiny fraction of matrix, fragment, and analyte ions. Depending on the laser pulse duration or pulse repetition frequency, there may be further interactions between the laser pulse and this plume. This would typically be true for nanosecond pulses in the visible and ultraviolet, and also for the train of FEL micropulses; in the latter case, the relaxation times of many non-diffusive processes are sufficiently short that succeeding pulses may excite ground-state species. From this intermediate state, ions are formed by physical and chemical mechanisms still to be determined and are extracted from the plume prior to detection. The measured ion spectra represent the final state of this complex process, and carry information only about the time-integrated evolution from the initial state through the formation of the ablation plume whence the ions are extracted long after all collision and relaxation processes are completed.

The conventional picture of UV-MALDI assumes that matrix ionization is the precursor to analyte ionization. Electronic excitation either of the matrix or of the ablation plume is presumed to lead to ion formation through such mechanisms as multiphoton ionization, energy pooling, thermal ion formation, disproportionation reactions, excited state proton transfer, desorption of preformed ions or phase transitions. Analyte ionization is then thought to follow via ion-molecule reactions between analyte and matrix in the ablation plume [4,6,35-38].

The "standard model" is founded on the well-established principles of resonant electronic excitation in molecules and excitonic processes in solutions and crystals. The matrix-excitation process in UV-MALDI can be represented schematically as follows:

$M + h\nu \rightarrow M^*$ *resonant excitation of a ground-state matrix molecule* (3.1)

An excited matrix molecule could then be further excited either by a second photon absorption event or by energy pooling:

$M^* + h\nu \rightarrow M^{**}$ *photoexcitation to a higher excited state* (3.2)

$M^* + M^* \rightarrow M^{**} + M$ *energy pooling to form a highly excited matrix molecule* (3.3)

If the energy of M** exceeds the matrix ionization potential (IP), then direct ionization can result:

$M^{**} \rightarrow M^+ + e^-$ (3.4)

If the energy of M** is less than the matrix IP then ionization may proceed by either collisional or photo-induced processes:

$M^{**} + M \rightarrow M^+ + M + e^-$ *collisional ionization of a highly excited state* (3.5)

$M^{**} + h\nu \rightarrow M^+ + e^-$ *photoionization of a highly excited matrix molecule* (3.6)

The final state in which the analyte ions are measured is reached by charge transfer from matrix to analyte:

$M^+ + A \rightarrow A^+ + M$ *analyte ionization by direct charge transfer* (3.7)

In many models a protonated matrix molecule is thought to be a likely precursor species:

$MH^+ + A \rightarrow AH^+ + M$ *Proton transfer* (3.8)

3.6. UV-MALDI: electronic excitation and ionization processes

The initial matrix excitation and ionization should be very different under femtosecond vs nanosecond irradiation as pulse intensities differ by more than four orders of magnitude. Hence femtosecond and nanosecond excitation in UV-MALDI should yield clear differences in mass spectra at comparable fluences if single-, multi- or multiple-photon processes directly influence analyte ionization either in the initial laser-solid interaction or the ablation plume.

The probability p for multiphoton excitation in the solid phase or the ablation plume is $p \propto \eta\sigma_{(k)}I^k$, where η is a quantum efficiency that includes all collisional or other mechanisms removing flux from the ionization channel, $\sigma_{(k)}$ is the k-photon cross section and I is the laser intensity. In our case, the irradiance of the 266 nm femtosecond pulse is 3×10^4 greater than that of the 266 nm nanosecond pulse when equal fluence pulses are used. If the direct precursor to

analyte ionization were a two-photon excitation, then, the ionization probability should be nearly a factor of 10^9 greater for femtosecond than for nanosecond excitation. (The existence of resonant intermediate excited states alters this simple picture somewhat.) If analyte ionization resulted directly from interactions with ionized matrix species in the solid phase, femtosecond excitation should also produce analyte ions much more efficiently. However, no dramatic enhancement of matrix or analyte ion yield is observed when femtosecond pulses are used instead of nanosecond pulses. Furthermore, there are no obviously distinguishable features arising from the two different time domains in the analyte mass spectra, the fluence threshold for ionization, the adduct intensity or the fragmentation patterns. This may simply be a manifestation of a rate-limited process due to the preponderance of neutral species in the ablation plume.

Figure 3.3(a)-(d) shows a comparison of UV-MALDI mass spectra using photon energies of 3.1, 3.7, and 4.7, and 4.7 eV, respectively. All spectra display a strong protonated angiotensin II mass peak and a weak Na adduct feature, while the low-mass region displays varying degrees of alkali metal adduction and fragmentation. If the relative ionization potentials, or proton affinities, of the matrix and/or analyte affected the efficiency of the processes described in Eqns. (3.7) and (3.8), excitation and ionization rates should depend strongly on wavelength, irradiance, and photon number density. For example, the ionization potential of gas-phase 2,5-DHB is 8.05 eV [35] and we can reasonably assume the solid-state IP is similar. Hence, three 337 nm photons or two 266 nm photons would be required to reach the IP of 8.05 eV. Such multiphoton ionization can be fairly efficient as the first excitation step is an allowed transition and there is a large density of higher-lying excited states. The single-photon excited state initially accessed by 337 nm absorption is the lowest singlet molecular state S_1 (3.47 eV), but 266 nm excitation accesses the next higher state, the S_2 threshold [35]. Excitation at 400 nm is well below the S_1 threshold and likely proceeds through a two-photon process. These three different routes to ionization should show strong dependence on wavelength, pulse duration, or both. Yet once again, the experimental data show little variation in relative analyte ion yield as a function of excitation mode, thus calling into question the role of ionized and excited matrix molecules in the final analyte ion distribution.

A proposed MALDI mechanism based on excited-state proton transfer (ESPT) [4,11] is attractive because the process requires only resonant single-photon excitation to produce the precursor to analyte ionization

$$M^* + A \rightarrow [M - H]^- + AH^+ \quad (3.9)$$

ESPT could possibly account for the efficiency of nanosecond UV-MALDI at the low fluences typical of MALDI. The matrix molecule is presumed to be much more acidic when electronically excited, leading to facile protonation of analyte molecules. However, the popular matrices are not known to be ESPT active, while some established ESPT molecules are poor matrices [6]. Thus the apparent similarity of analyte mass spectra presented in Figs. 3.1-3.3 is a further argument against ESPT as an important mechanism in MALDI given the wide range of initial excited state distributions and ionization densities produced by the various ultraviolet laser sources.

The question of laser-induced ionization in the evolving ablation plume can be addressed by comparing femtosecond and nanosecond UV-MALDI experiments. In nanosecond UV-MALDI, ablation begins while the laser pulse is still irradiating the surface, as can be inferred from picosecond double-pulse experiments on wide bandgap crystals such as Al_2O_3 [39] and $LiNbO_3$ [40]. The effect of laser irradiation on the expanding plume is not well understood, but some excitation of matrix and other molecules is generally presumed. Laser excitation and ionization of the plume is also an attractive hypothesis for nanosecond laser ionization because of the large neutral yield in MALDI [41]. The energy of a femtosecond laser pulse, on the other hand, is absorbed completely prior to any movement of the matrix. Moreover, in femtosecond UV-MALDI, neither photoacoustic or thermomechanical effects on the matrix are important, since the nominal 120 fs laser pulse is absorbed before either thermal diffusion ($\tau \approx 10$ ns) or acoustic wave generation ($\tau \approx 20$ ps) occurs [42].

If a laser-plume ionization process were important, there might be an optimal pulse duration for maximal analyte ion yield, as observed in recent two-pulse experiments [43]. However, this pulse duration should in principle be correlated with the excited-state lifetime of the matrix, a quantity that varies considerably among effective UV matrices [43-45]. For example, DHB has only short-lived excited states ($\tau \approx 5$ ns) while 3-HPA fluoresces for tens of microseconds. Yet the effectiveness of both DHB and 3-HPA as matrices is well known. All

these factors suggest that an excited-state-mediated process is not a dominant analyte ionization channel in UV-MALDI.

3.7. IR-MALDI: vibrational excitation and ionization processes

There is no 'standard model' for infrared MALDI. In fact, in the earliest days of MALDI experiments, it was presumed that IR photons had insufficient energy to initiate the processes of desorption and ionization. Nevertheless, in 1990 the Hillenkamp group demonstrated IR-MALDI at 2.94 μm and 10.6 μm wavelengths [46]. Since that time, several groups have confirmed the effectiveness of IR-MALDI over a range of wavelengths and pulse durations.

In IR-MALDI, initial energy deposition proceeds through rovibronic excitation. At least in simple materials, the ablation mechanism depends strongly on the local density of vibrational excitation [47]. Subsequent ionization mechanism(s) is(are) generally regarded as unknown, although evidence for a multiphoton ladder-climbing excitation process is supported by a recent IR experiment [48]. However, between 20 and 70 photons would be required to ionize a single matrix molecule directly, a wildly improbable prospect. Moreover, since the IR-MALDI analyte threshold intensities are generally only one order of magnitude greater than in UV-MALDI, direct multiphoton ionization seems somewhat unlikely under nanosecond IR laser excitation.

The present experiments showing that IR- and UV-MALDI ion spectra strongly resemble each other are perhaps the best evidence that mass spectra by themselves convey little information on the mechanistic details of ablation and ionization. This is because the IR excitation, ablation and ionization mechanisms must by nature be very different from their counterparts in UV-MALDI, not only because of deeper penetration depth (the common explanation for differences), but also because the character of the initial laser-solid interactions depends on resonant vs non-resonant excitation.

3.8. Can a single model explain UV- and IR-MALDI?

Experiments from several groups show nearly identical mass spectra for many wavelengths [29,30,46] at nanosecond pulse durations. These have been interpreted to mean that there is a single MALDI mechanism, independent of the specific mode of excitation. The arguments are not without merit; certainly some of the experimental data are consistent with the

proposition that an effective MALDI process may require only the rapid deposition of a threshold energy density into the matrix.

One mechanism that could satisfy the constraints of a unified model would be a phase transition leading to matrix ablation [30]. In such a phase change, matrix molecules and the embedded analytes would be quickly transformed into a fluid-like environment. The enhanced ion mobility in this liquid-like phase would allow the charges to pool (e.g., by adduction of H^+), subsequently leading to electrostatic repulsion that ejects ions into the gas phase in a rapid vaporization process. Variations on this phase change model with similar consequences would include the explosive solid- to gas-phase transition, the so called 'phase explosion', and spallation. In the high-density region of ablated or spalled material, electrons, neutrals, protons and ions are all likely to be present. The interaction of these species in close proximity could lead to ion formation through low-energy secondary electron attachment, collisions, or other charge transfer processes, leading to formation of cations, anions and dipole-bound anions [49]. Indeed, in IR-laser-initiated explosive vaporization in fused silica, there is a dramatic increase in positive-ion production at the phase explosion threshold [50].

Alternatively, the similarity of the mass spectra could be the result of secondary collisional processes occurring in the expanding plume. If equilibrium conditions are present in the plume, then the species with the highest proton affinity will preferentially abstract free charges or benefit from charge transfer from species with weaker proton affinities [51]. Thus regardless of the initial ion species generated by diverse excitation pathways, the surviving ions ions will instead reflect plume processes.

However, it is not clear that a single mechanism is at work in either UV- or IR-MALDI. In UV-MALDI, there is strong evidence for both thermal and non-thermal ion generation in a 'typical' dried droplet experiment [52]; similar results have also been seen in IR-MALDI [48]. In "ultrathin" sample preparations, the prompt (non-thermal) ion fraction seems to dominate the velocity distribution [52]; in this case, one would expect to see significant differences between nanosecond and femtosecond MALDI at UV wavelengths. All of these complications suggest that a single mechanism is unlikely – even before one takes into account differences in analyte species.

3.9. Conclusion

A wide variety of excitation schemes distinct in pulse duration and wavelength, from ultraviolet to infrared and from femtosecond to nanosecond duration, have produced strikingly similar analyte mass spectra in the MALDI experiments presented here. A direct experimental correlation between excitation source and final ion yield is not evident. This is consistent with the idea that secondary reactions in UV-MALDI, predictable from chemical thermodynamics, may be so dominant that the primary ionization events are simply not reflected in the final ion distribution [51]. The extremely broad range of wavelengths and pulse durations used in the present experiment is the strongest confirmation to date that this is the case. Neither the initial matrix ionization state, the laser-solid interaction mechanism, nor the pathway from electronic or vibrational excitation to the laser ablation plume appears to be reflected in analyte ion spectra in UV- or IR-MALDI; even the matrix and fragment ion distributions show little correlation with the mode of laser excitation. It also does not appear that multiphoton ionization or excitation in the laser-solid interaction or in the ablation plume plays much of a role in the matrix-analyte systems explored here.

However, lest this be interpreted as an argument in favor of a common MALDI mechanism, we note that all the present results are derived for a single matrix material and with small analytes known to be observable under these conditions. With few exceptions this model system or ones strongly resembling it constitute the principal body of evidence adduced in support of a unified mechanistic model for MALDI. Since the present experiments show insignificant differences between analyte ion mass spectra for systems known from first principles to be initiated by very different mechanisms, this work indicates strongly that mass spectra *by themselves* are not reliable guides to the operative MALDI mechanisms. Once the ablation plume – the intermediate state between laser-material interaction and ion detection – has reached thermal equilibrium, the outcome of the process is effectively the same *for analyte ions that manage to survive the initial excitation*, *formation and decay process*.

We propose that the operative physical and chemical mechanisms will only be identified by definitive studies of the elusive intermediate state from which the MALDI ion spectra originate. At the very least, careful studies of ion velocity distributions will have to assume much greater priority [53]. In particular, the comparative ion velocities of infrared- and ultraviolet-laser generated ions, about which there is some uncertainty, should be measured from

similar systems. Furthermore, for the specific case of IR-MALDI, ion velocities for strongly *vs.* weakly resonant absorption modes may prove instructive as the mechanisms of ablation are likely to change with absorption cross-section. In these studies, the use of multiple laser frequencies, continuously tunable lasers, and ultrafast as well as nanosecond pulse durations will be indispensable, as they will create different physical states of stress and thermal confinement. Perhaps even more important, given the dominance of neutral matrix and analyte molecules and fragments at every stage of the laser-solid and laser-plume interactions, may be the characterization of the kinetics and dynamics of the neutral species that so far go mostly unobserved in MALDI experiments.

BIBLIOGRAPHY

[1] G. S. Edwards, D. Evertson, W. Gabella et al., IEEE J. Sel. Top. Quantum Electron. **2**, 810 (1996).

[2] M. Karas, D. Bachmann, U. Bahr, and F. Hillenkamp, International Journal of Mass Spectrometry and Ion Processes **78**, 53 (1987).

[3] M. Karas, U. Bahr, A. Ingendoh et al., Analytica Chimica Acta **241** (2), 175 (1990).

[4] H. Ehring, M. Karas, and F. Hillenkamp, Org. Mass Spectrom. **27** (4), 472 (1992).

[5] F. Hillenkamp, M. Karas, R. C. Beavis, and B. T. Chait, Analytical Chemistry **63** (24), A1193 (1991).

[6] Renato Zenobi and Richard Knochenmuss, Mass Spectrometry Reviews **17**, 337 (1998).

[7] William R. Wilkinson, Arkady I. Gusev, Andrew Proctor, Marwan Houlla, and David M. Hercules, Fresenius Journal of Analytical Chemistry **357**, 241 (1997).

[8] X. D. Tang, M. E. Sadeghi, Z. Olumee et al., Analytical Chemistry **68** (21), 3740 (1996).

[9] R. M. Whittal, M. M. Palcic, O. Hindsgaul, and L. Li, Analytical Chemistry **67** (19), 3509 (1995).

[10] S. Jespersen, W. M. A. Niessen, U. R. Tjaden, and J. Vandergreef, Journal of Mass Spectrometry **30** (2), 357 (1995).

[11] David J. Harvey, Mass Spectrometry Reviews **18** (6), 349 (1999).

[12] Michel W. F. Nielen, Mass Spectrometry Reviews **18** (5), 309 (1999).

[13] Steven C. Goheen, Karen L. Wahl, James A. Campbell, and Wayne P. Hess, J. Mass Spectrom. **32** (8), 820 (1997).

[14] Wayne P. Hess, Hee K. Park, Oguz Yavas, and R. F. Haglund Jr., Applied Surface Science **127-129**, 235 (1998).

[15] S. Jespersen, W. M. A. Niessen, U. R. Tjaden et al., in *Mass Spectrometry in Biological Sciences*, edited by S. A. Carr (Humana Press, Totowa, NJ, 1996), pp. 217.

[16] M. M. Siegel, K. Tabei, R. S. Tsao et al., Journal of Mass Spectrometry **34** (6), 661 (1999).

[17] C. Menzel, S. Berkenkamp, and F. Hillenkamp, Rapid Communications in Mass Spectrometry **13** (1), 26 (1999).

[18] S. Berkenkamp, F. Kirpekar, and F. Hillenkamp, Science **281** (5374), 260 (1998).

[19] R. Cramer, R. F. Haglund, and F. Hillenkamp, International Journal of Mass Spectrometry **169/170**, 51 (1997).

[20] P. Demirev, A. Westman, C. T. Reimann et al., Rapid Communications in Mass Spectrometry **6** (3), 187 (1992).

[21] K. Dreisewerd, M. Schurenberg, M. Karas, and F. Hillenkamp, International Journal of Mass Spectrometry and Ion Processes **154** (3), 171 (1996).

[22] A. Meffert and J. Grotemeyer, Berichte Der Bunsen-Gesellschaft-Physical Chemistry Chemical Physics **102** (3), 459 (1998).

[23] M. J. Dale, R. Knochenmuss, and R. Zenobi, Analytical Chemistry **68** (19), 3321 (1996).

[24] Jay D. Sheffer and Kermit K. Murray, Rapid Communications in Mass Spectrometry **12** (22), 1685 (1998).

[25] P. Kraft, S. Alimpiev, E. Dratz, and J. Sunner, Journal of the American Society for Mass Spectrometry **9** (9), 912 (1998).

[26] R. Cramer and A. L. Burlingame, Rapid Communications in Mass Spectrometry **14** (2), 53 (2000).

[27] M. L. Vestal, P. Juhasz, and S. A. Martin, Rapid Communications in Mass Spectrometry **9** (11), 1044 (1995).

[28] R. S. Brown and J. J. Lennon, Analytical Chemistry **67** (21), 3990 (1995).

[29] S. F. Niu, W. Z. Zhang, and B. T. Chait, Journal of the American Society for Mass Spectrometry **9** (1), 1 (1998).

[30] X. J. Chen, J. A. Carroll, and R. C. Beavis, Journal of the American Society for Mass Spectrometry **9** (9), 885 (1998).

[31] M. R. Papantonakis, J. Kim, W. P. Hess, and R. F. Haglund, Journal of Mass Spectrometry **37** (6), 639 (2002).

[32] A. Mele and L. Malpezzi, Journal of the American Society for Mass Spectrometry **11** (3), 228 (2000).

[33] V. Horneffer, K. Dreisewerd, H. C. Ludemann et al., International Journal of Mass Spectrometry **187**, 859 (1999).

[34] Christoph Menzel, Klaus Dreisewerd, Stefan Berkenkamp, and Franz Hillenkamp, International Journal of Mass Spectrometry **207** (1-2), 73 (2001).

[35] V. Karbach and R. Knochenmuss, Rapid Communications in Mass Spectrometry **12** (14), 968 (1998).

[36] K. Breuker, R. Knochenmuss, and R. Zenobi, Journal of the American Society for Mass Spectrometry **10** (11), 1111 (1999).

[37] M. Gluckmann and M. Karas, Journal of Mass Spectrometry **34** (5), 467 (1999).

[38] Michael Karas, Matthias Gluckmann, and Jurgen Schafer, J. Mass Spectrom. **35** (1), 1 (2000).

[39] A. V. Hamza, R. S. Hughes, L. L. Chase, and H. W. H. Lee, Journal of Vacuum Science & Technology B **10** (1), 228 (1992).

[40] S. Preuss, M. Spath, Y. Zhang, and M. Stuke, Applied Physics Letters **62** (23), 3049 (1993).

[41] C. D. Mowry and M. V. Johnston, Rapid Communications in Mass Spectrometry **7** (7), 569 (1993).

[42] L. V. Zhigilei and B. J. Garrison, Applied Physics Letters **74** (9), 1341 (1999).

[43] X. D. Tang, M. Sadeghi, Z. Olumee, and A. Vertes, Rapid Communications in Mass Spectrometry **11** (5), 484 (1997).

[44] R. Knochenmuss, F. Dubois, M. J. Dale, and R. Zenobi, Rapid Communications in Mass Spectrometry **10** (8), 871 (1996).

[45] H. Ehring and B. U. R. Sundqvist, Journal of Mass Spectrometry **30** (9), 1303 (1995).

[46] A. Overberg, M. Karas, U. Bahr, R. Kaufmann, and F. Hillenkamp, Rapid Communications in Mass Spectrometry **4** (8), 293 (1990).

[47] D. R. Ermer, M. R. Papantonakis, M. Baltz-Knorr, D. Nakazawa, and R. F. Haglund, Applied Physics A-Materials Science & Processing **70** (6), 633 (2000).

[48] D. R. Ermer, M. Baltz-Knorr, and R. F. Haglund, Journal of Mass Spectrometry **36** (5), 538 (2001).

[49] M. A. Johnson, M. L. Alexander, and W. C. Lineberger, Chemical Physics Letters **112** (4), 285 (1984).

[50] R. F. Haglund and D. R. Ermer, Applied Surface Science **168** (1-4), 258 (2000).

[51] R. Knochenmuss, A. Stortelder, K. Breuker, and R. Zenobi, Journal of Mass Spectrometry **35** (11), 1237 (2000).

[52] G. R. Kinsel, R. D. Edmondson, and D. H. Russell, Journal of Mass Spectrometry **32** (7), 714 (1997).

[53] G. R. Kinsel, M. E. Gimon-Kinsel, K. J. Gillig, and D. H. Russell, Journal of Mass Spectrometry **34** (6), 684 (1999).